Stretching Response of Discrete Semiflexible Polymers

L. Livadaru,[†] R. R. Netz,*[,‡,§] and H. J. Kreuzer[†]

Department of Physics, Dalhousie University, Halifax, NS, Canada, B3H 3J5, Max-Planck-Institute for Colloids and Interfaces, 14424 Potsdam, Germany, and Sektion Physik, Ludwig-Maximilians-Universität, Theresienstrasse 37, 80333 München, Germany

Received May 16, 2002; Revised Manuscript Received March 21, 2003

ABSTRACT: We demonstrate that semiflexible polymer chains (characterized by a persistence length ℓ) made up of discrete segments or bonds of length b show at large stretching forces a crossover from the standard wormlike chain (WLC) behavior to a *discrete-chain* (DC) behavior. In the DC regime, the stretching response is independent of the persistence length and shows a different force dependence than in the WLC regime. We perform extensive transfer-matrix calculations for the force-response of a freely rotating chain (FRC) model as a function of varying bond angle γ (and thus varying persistence length) and chain length. The FRC model is a first step toward the understanding of the stretching behavior of synthetic polymers, denatured proteins, and single-stranded DNA under large tensile forces. We also present scaling results for the force response of the *elastically jointed chain* (EJC) model, that is, a chain made up of freely jointed bonds that are connected by joints with some bending stiffness; this is the discretized version of the continuum WLC model. The EJC model might be applicable to stiff biopolymers such as double-stranded DNA or Actin. Both models show a similar crossover from the WLC to the DC behavior, which occurs at a force $f/k_BT \sim \ell/b^2$ and is thus (for polymers with a moderately large persistence length) in the piconewton range probed in many AFM experiments. We also give a heuristic simple function for the force−distance relation of a FRC, valid in the global force range, which can be used to fit experimental data. Our findings might help to resolve the discrepancies encountered when trying to fit experimental data for the stretching response of polymers in a broad force range with a single effective persistence length.

I. Introduction

Since single-molecule manipulation techniques have become available, large amounts of experimental data have been accumulated on the response of polymers to stretching forces.[1] Using magnetic beads, the extension of single DNA molecules has been determined in the force range of 100 fN to 10 pN[2] and found to be well described by the wormlike chain (WLC) model.[3−7] Atomic-force microscopy allows forces to be measured in the range from 10 pN up to covalent-bond breakage at a few nanonewtons and has been used to study DNA,[8] proteins,[9] polysaccharides,[10] synthetic neutral polymers,[11] and synthetic polyelectrolytes.[12,13] In all theoretical treatments using the WLC model, a continuous description was employed; i.e., the chain was considered as a homogeneous line with no microscopic structure. The only parameter appearing in the WLC model is the persistence length ℓ, which measures the length over which the chain loses its orientational correlation and, as a heuristic parameter, takes the microscopic details of the real chain into account.

However, real chains are not structureless, continuous lines. Synthetic polymers with saturated carbon backbones consist of C−C bonds of a length $b \approx 0.15$ nm which rotate at a more or less fixed bond angle of $\gamma \approx 70°$. This structure forms the conceptual basis of the so-called freely rotating chain (FRC) model, as depicted in Figure 1a, which will be treated in the presence of a stretching force in this article (in the present paper, we leave aside the fact that the bond angle and the bond length itself are not fixed but fluctuate and that the bond rotation is subject to a rotational potential due to interactions between chemical groups located at further-nearest neighbor carbon atoms). The same discrete backbone structure, albeit more complicated, is present for denatured proteins, single-stranded DNA, or polysaccharides. On the other hand, many biopolymers cannot

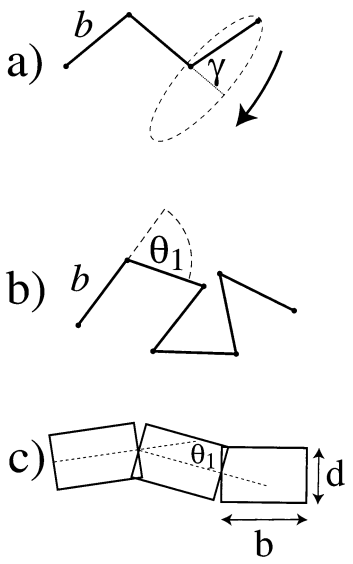

Figure 1. Different chain models used in this article: (a) freely rotating chain (FRC) model characterized by bonds of fixed length b which are connected at fixed bond angles γ but arbitrary torsional angles; (b) elastically jointed chain (EJC) model with bonds of fixed length b and arbitrary bond angles θ_i which are connected by joints with some bending stiffness; (c) model for the calculation of the bending stiffness of a biopolymer made up of globular sections of thickness d and length b.

* To whom correspondence should be addressed at the Ludwig-Maximilians-Universität.
† Dalhousie University.
‡ Max-Planck-Institute for Colloids and Interfaces.
§ Sektion Physik, Ludwig-Maximilians-Universität.

10.1021/ma020751g CCC: $25.00
Published on Web 04/25/2003

be described as a chain with rotating bonds of fixed length, since they consist of helical structures made up of two or more interwound macromolecules (such as double-stranded DNA or collagen) or of objects assembled from globular proteins (like actin or tubulin). Although the elastic behavior of such structures is more complicated and includes in addition to stretching and bending modes also torsional modes,[14] it should be clear that at small length scales the discrete nature of the building blocks comes into play, be it the individual stacked base pairs in the case of ds DNA or the stacked globular proteins in the case of actin. For such biopolymers and in the absence of torsional constraints, we propose the *elastically jointed chain* (EJC) model which consists of stiff segments of length b which are connected by elastic joints with some bending stiffness, as schematically depicted in Figure 1b. The length b can be tentatively associated with the base pair stacking distance for ds DNA or the size of a globular protein for actin, and the bending stiffness follows from the lateral size of the building blocks and the strength of the bonds stabilizing the polymer structure (as is discussed in Appendix A).

Both models, the freely rotating chain model, which is treated numerically by transfer-matrix techniques in this paper, and the elastically jointed chain model, which is amenable to scaling arguments, show that at a force larger than $f/k_BT \sim \ell/b^2$, one enters the discrete-chain regime, in which the chain length R_z divided by the contour length L obeys $R_z/L \simeq 1 - (cbf/k_BT)^{-1}$ and replaces the WLC behavior observed for smaller forces, $R_z/L \simeq 1 - (4\ell f/k_BT)^{-1/2}$. Note that the force response in the DC regime is similar but, due to the presence of the constant c which depends on the architectural details of the chain, not identical to the behavior of a freely jointed chain. This deviation from the WLC behavior is due to the fact that at increasing forces the dominant chain fluctuations probe progressively smaller length scales and above the crossover force become sensitive to the discrete nature of the semiflexible chain. For a synthetic polymer chain with a persistence length of e.g. $\ell = 0.6$ nm and a bond length $b = 0.15$ nm, we obtain a crossover force of $f \simeq k_BT\ell/b^2 \approx 100$ pN, which is right in the middle of the force range that is studied in typical AFM experiments (we have used the fact that $k_BT \approx 4$ pN nm).[12,13] Experimentally, it has indeed been found that the WLC chain model is not able to satisfactorily fit the stretching data of poly(vinylamine) (a synthetic polymer with a fully saturated carbon-backbone architecture) over the entire force range from 10 pN to more than 500 pN.[13] For polymers with a larger persistence length (for example DNA or other biopolymers), the crossover occurs at a higher force where these polymers are typically unstable. The crossover to the DC regime is therefore most relevant for synthetic polymers and biopolymers with a rather small persistence length.

In section II, we present our scaling results for the elastically jointed chain model, leading to a global scaling diagram which features three different stretching regimes as a function of the applied force and the persistence length, namely the linear force regime, the WLC regime, and the discrete chain (DC) regime. In Appendix A, we also explain how to estimate the bending energy of a biopolymer made up of globular building blocks, as shown in Figure 1c, which gives a simple scaling relation between the persistence length of such biopolymers and the volume of the building blocks. In section III, we present our transfer matrix results for the freely rotating chain. These numerical results confirm the scaling results. Section IV is devoted to a brief discussion and outlook, where we also present an empirical function which describes the stretching response well in the entire force range and covers the linear regime, the WLC regime, and the crossover to the DC regime. This fitting function depends on both relevant length scales, namely the persistence length and the bond length, and might prove useful for fitting experimental data.

II. Stretching Response of the Elastically Jointed Chain: Scaling Approach

Let us consider a chain made up of bonds of fixed length b with in principle arbitrary bond angles θ_i as depicted in Figure 1b. In the FJC model, these bond angles fluctuate freely, at no energy penalty, in the FRC model the bond angles are all fixed to a value $\theta_i = \gamma$. In the elastically jointed chain (EJC) model each bond angle is subject to a periodic potential of the strength ϵ so that the total energy of the chain is

$$\frac{H}{k_BT} = \epsilon \sum_i (1 - \cos\theta_i) \tag{1}$$

This energy expression indeed follows from a discretization of the continuous wormlike chain energy,

$$\frac{H}{k_BT} = \frac{\ell}{2}\int \mathrm{d}s\, \dot{\mathbf{t}}^2(s) \tag{2}$$

where $\mathbf{t}(s)$ is the normalized tangent vector, s is the contour length, and ℓ denotes the persistence length of the chain. Replacing the integral by a discrete sum over segments of length b, the differential $\dot{\mathbf{t}}(s) = \partial\mathbf{t}(s)/\partial s$ is approximated by the difference $\dot{\mathbf{t}}(s) \approx (\mathbf{t}_{i+1} - \mathbf{t}_i)/b$, and the energy of the discretized WLC becomes

$$\frac{H}{k_BT} = \frac{\ell b}{2}\sum_i \left(\frac{\mathbf{t}_i - \mathbf{t}_{i+1}}{b}\right)^2 \tag{3}$$

Noting that $\mathbf{t}_i^2 = 1$ and $\mathbf{t}_i \cdot \mathbf{t}_{i+1} = \cos\theta_i$, eq 1 follows, and the constant ϵ is related to the persistence length via $\epsilon = \ell/b$.

The angular correlations between two neighboring bonds is characterized by the expectation value $\langle\cos\theta_i\rangle$, which can from the Hamiltonian equation, eq 1, be exactly calculated to be

$$\langle\cos\theta_i\rangle \equiv g(\epsilon) = \frac{1 - \epsilon^{-1} + \mathrm{e}^{-2\epsilon}(1 + \epsilon^{-1})}{1 - \mathrm{e}^{-2\epsilon}} \tag{4}$$

with the limiting behavior

$$g(\epsilon) \simeq \begin{cases} \epsilon/3 & \text{for } \epsilon \ll 1 \\ 1 - \epsilon^{-1} & \text{for } \epsilon \gg 1 \end{cases} \tag{5}$$

Not surprisingly, as the joints become stiffer, that is as ϵ increases, the angular correlations become more pronounced and $g(\epsilon)$ approaches unity, whereas for decreasing joint stiffness the correlations gradually vanish. In the absence of external forces, and since the chain is a Markov chain with nearest-neighbor correlations only, the correlations between any two bonds obey the formula

$$\langle \mathbf{t}_j \cdot \mathbf{t}_{j+i} \rangle = \langle \cos \theta_i \rangle^i = g(\epsilon)^i \tag{6}$$

By exponentiation, this can be brought into the more appealing form

$$\langle \mathbf{t}_j \cdot \mathbf{t}_{j+i} \rangle = \mathrm{e}^{-i\ (\ln g^{-1}(\epsilon))} = \mathrm{e}^{-ib/\ell} \tag{7}$$

where the persistence length of the EJC model is given by

$$\ell = \frac{b}{\ln g^{-1}(\epsilon)} \tag{8}$$

with the limiting behavior

$$\ell \simeq \begin{cases} b/\ln(3/\epsilon) & \text{for } \epsilon \ll 1 \\ b\epsilon & \text{for } \epsilon \gg 1 \end{cases} \tag{9}$$

The persistence length in the limit of stiff bonds is indeed the one that follows from the discretization of the WLC model (see the discussion after eq 3), as expected, since for stiff bonds the discretization can be viewed as an accurate approximation to the continuum model; for soft bonds, on the other hand, there are pronounced deviations. For the following scaling arguments, we will be mostly interested in the stiff-bond limit. In Appendix A, we propose a simple model for the stiffness of biopolymers which relates the joint-bending modulus ϵ with the volume of a polymer building block and the strength of the inter-block interactions that stabilize the biopolymer. The main point here is that the bending modulus ϵ turns out to be proportional to the volume of the globular building blocks.

If an external force is applied to a WLC, the extension along the direction of the force, R_z, increases. For small forces, the extension (rescaled by the contour length L) obeys the standard result for Gaussian chains

$$\frac{R_z}{L} \simeq \frac{fa}{3k_\mathrm{B}T} \tag{10}$$

if for the Kuhn length a the relation $a = 2\ell$ is used. The latter relation follows by comparing the unperturbed mean-squared radius for a long (i.e., $L \gg \ell$) WLC, which is $R^2 = 2\ell L$, with the definition of the Kuhn length, $R^2 = aL$. The corresponding large-force relation for the WLC is[15]

$$\frac{R_z}{L} = 1 - \left(\frac{4f\ell}{k_\mathrm{B}T}\right)^{-1/2} \tag{11}$$

The crossover between these two predictions occurs at a force $f\ell \sim k_\mathrm{B}T$. An interpolation formula for the WLC stretching by Marko and Siggia[6] is

$$\frac{f\ell}{k_\mathrm{B}T} = \frac{R_z}{L} + \frac{1}{4(1 - R_z/L)^2} - \frac{1}{4} \tag{12}$$

and has a maximum error of 10% in the intermediate force regime, but accurately represents the small and large force regimes as given by eqs 10 and 11. A different interpolation formula has been suggested,[16] and the range of validity of various fitting functions has been thoroughly investigated.[17] For the present purposes, eq 12 is of sufficient accuracy.

If a force is applied to the EJC model, we expect the stretching response of the chain in the large force regime to be represented by eq 11 up to a force threshold at which the orientation effect of the external force exceeds the orientation effect due to the interaction of one bond with its neighboring, correlated bonds. In other words, for very large forces, the fact that the bonds are connected by stiff joints becomes irrelevant, and they act like freely jointed bonds. The force-extension relation for the FJC is analytically known for all forces, namely the Langevin function[18]

$$\frac{R_z}{L} = \coth\left(\frac{fb}{k_\mathrm{B}T}\right) - \left(\frac{fb}{k_\mathrm{B}T}\right)^{-1} \tag{13}$$

In the large-force regime, $fb/k_\mathrm{B}T \gg 1$, one obtains

$$\frac{R_z}{L} \simeq 1 - \left(\frac{fb}{k_\mathrm{B}T}\right)^{-1} \tag{14}$$

while for small forces the linear regime eq 10 is recovered with the Kuhn length given by $a = b$. By comparing the large force responses of the WLC model, eq 11, with the FJC model, eq 14, the crossover between the two regimes is expected to occur at a force

$$\frac{f}{k_\mathrm{B}T} \simeq \frac{\ell}{b^2} \tag{15}$$

For smaller forces, the typical WLC behavior is expected; for larger force, one enters into the discrete chain (DC) regime in which the large-force prediction of the FJC model becomes valid. The different regimes encountered as a function of applied stretching force and persistence length are summarized in the scaling diagram shown in Figure 2. As a function of increasing force one typically observes the linear force regime (eq 10) for small forces, the large-force part of the WLC model (eq 11) for intermediate forces, and the large-force part of the FJC model (eq 14) for large forces. Note that for rather flexible chains, i.e., if the persistence length is of the same order as the bond length, the intermediate WLC regime is missing and one obtains a behavior similar to the FJC model for all forces. Note that the stretching behavior in the DC regime for the FRC model differs quantitatively (by a prefactor) from the response of the EJC model (as we will see in the following section on the FRC model). This shows that the stretching behavior in the DC regime depends sensitively on the detailed architecture of the underlying chain model.

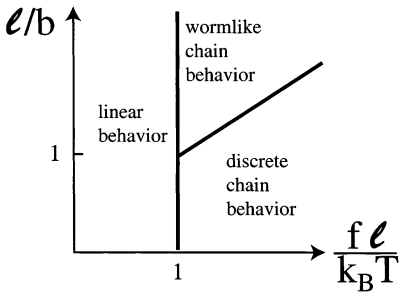

Figure 2. Schematic phase diagram for the stretching response of a discrete semiflexible chain, featuring a linear regime with a force response given by eq 10, a wormlike chain (WLC) regime with a response given by eq 11, and the discrete chain (DC) regime where eq 14 is valid. The axes are logarithmic, and the transition between the WLC and DC regimes is given by eq 15.

A more physical argument for the crossover to the DC regime involves the so-called deflection length λ, which is the correlation length along a semiflexible polymer.[19] For a semiflexible polymer under tensile force, the deflection length is given by

$$\lambda \sim \left(\frac{f}{k_B T \ell}\right)^{-1/2} \tag{16}$$

For a deflection length larger than the bond length b, the discreteness is irrelevant, and the stretching response should be given by that of a WLC model. However, if the deflection length becomes smaller than the bond length, the concept of a semiflexible chain breaks down, and the bonds are decoupled from each other, being described by a FJC model. The crossover is therefore predicted to occur at $\lambda \sim b$, which, with the formula in eq 16, leads to the same crossover force as already presented in eq 15.

As the main result from our scaling analysis, it is suggested that the stretching behavior of a discrete WLC model deviates for large forces from the continuum model, giving rise to a new regime with a very different scaling behavior. For a DNA chain with a persistence length of $\ell \approx 30$ nm and a bond length which one might associate with the base-pair stacking distance, $b \approx 0.34$ nm, the crossover is predicted to occur at a force of roughly a nanonewton. Since at these large forces the double-stranded structure is instable, this crossover is not relevant for DNA as such. On the other hand, it is relevant for biopolymers with a smaller persistence length, such as ss DNA, denatured proteins, polysaccharides, and also synthetic polymers. Since these polymers might to a first approximation be described by the FRC model, we will in the next section perform a detailed numerical analysis of the stretching behavior of this model. In the present formulation, we leave out the important effects of torsional potentials, which will be covered in a later publication. As will be discussed in more detail in the Discussion section, such refinements do not change the main conclusions regarding the existence of the discrete-chain regime.

III. Stretching Response of the FRC Model

The freely rotating chain (FRC) model consists of segments of the same length b while the bond angle between two neighboring segments has the fixed value γ as depicted in Figure 1a. Although it is a conceptually simple model, the statistical mechanical treatment is nontrivial and can be carried out analytically only to a certain extent. The behavior of the FRC model in the absence of an external force is summarized in the classical book of Flory[20] as well as in the more recent text of Grosberg.[21] A theoretical study of the FRC model using Green's functions methods was performed by Kostrowicki and Scheraga,[22] but their results were restricted to the end-to-end distribution function only. For the investigation of the response of a FRC to an external force, we therefore resort in this section to numerical transfer-matrix techniques.

First, we present a compilation of some of the classical results for the FRC. The mean squared end-to-end distance of a FRC consisting of N bonds in the absence of an external force is exactly given by

$$\langle R^2 \rangle = Nb^2\left(\frac{1+\cos\gamma}{1-\cos\gamma} - \frac{2\cos\gamma}{N}\frac{[1-(\cos\gamma)^N]}{(1-\cos\gamma)^2}\right) \tag{17}$$

which, in the infinite chain limit $N \to \infty$, becomes

$$\langle R^2 \rangle = Nb^2\frac{1+\cos\gamma}{1-\cos\gamma} \tag{18}$$

From the definition of the effective monomer size or Kuhn length a

$$\langle R^2 \rangle = La \tag{19}$$

where L is the contour length of the polymer, which for the FRC model is given by

$$L = Nb\cos(\gamma/2) \tag{20}$$

we obtain from eq 18 that the Kuhn length is in the infinite-chain limit given by

$$a = b\frac{1+\cos\gamma}{(1-\cos\gamma)\cos(\gamma/2)} \tag{21}$$

Since the angular correlation between two neighboring bonds is given by $\langle \mathbf{t}_i \cdot \mathbf{t}_{i+1} \rangle = \cos\gamma$, a derivation similar to the one leading to eq 8 yields for the persistence length of the FRC model

$$\ell = b\frac{\cos(\gamma/2)}{|\ln(\cos\gamma)|} \tag{22}$$

For small stretching forces $f/k_B T \ll 1/\ell$, scaling predicts the response of the FRC to be given by the linear force−distance relation in eq 10 valid for Gaussian chains if the correct value for the Kuhn length a in eq 21 is used (an expectation which will be confirmed by our numerical results). For larger forces, one expects deviations from the linear behavior, and in fact, we will see that for forces

$$1/\ell < f/k_B T < \ell/b^2 \tag{23}$$

the strong stretching prediction for the WLC model is recovered, eq 11, while for even larger forces $\ell/b^2 < f/k_B T$ a behavior similar (but not identical) to the strong-stretching prediction of the FJC model, eq 14, is obtained.

A. Transfer-Matrix Technique. Let us consider a FRC with bond angle γ under the action of a force f. We are interested in $G_i(\theta)$, the probability distribution function (or Green's function) of the ith segment of the chain, which measures the probability to find this segment at a certain angle θ with respect to the direction of the applied force. The geometry of this problem is schematically shown in Figure 3a. The Green's function of the $(i+1)$th segment is determined by the integral equation

$$G_{i+1}(\theta) = e^{fb\cos(\theta)/k_B T}\int d\theta'\, G_i(\theta')\mathbf{T}(\theta,\theta') \tag{24}$$

where $\mathbf{T}(\theta,\theta')$ is the transfer operator characterizing the geometrical constraints of finding the segment $(i+1)$ at an angle θ if segment i is at an angle θ'. It is given by

$$\mathbf{T}(\theta,\theta') = \int_0^{2\pi} d\phi\,\delta[\theta' - h(\theta,\phi)] \tag{25}$$

where ϕ is the dihedral angle between the planes spanned (i) by the two bonds and (ii) by the first bond

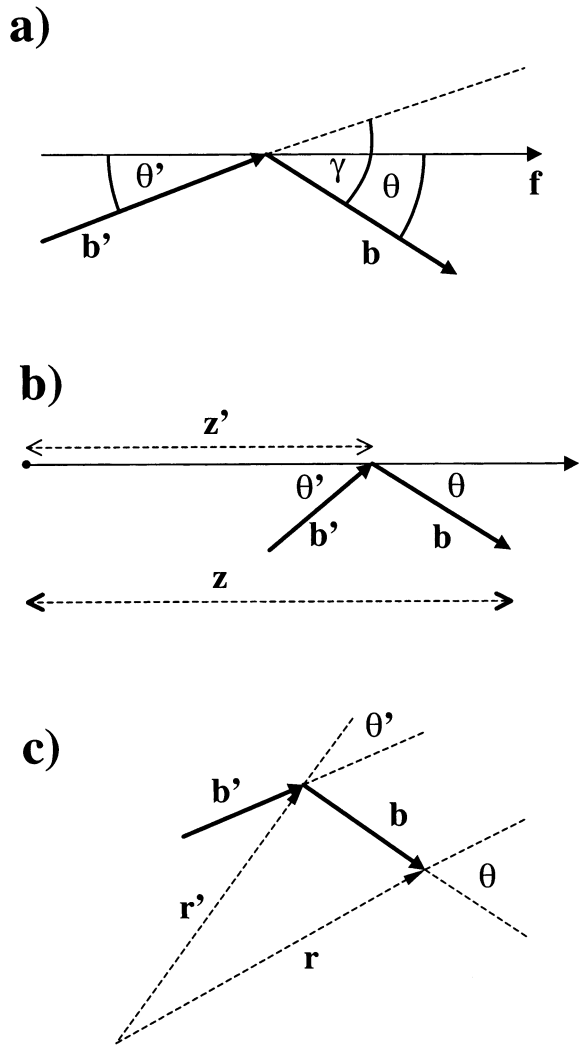

Figure 3. Schematic representation of the coordinates used in the various transfer-matrix schemes: (a) for the fixed-force ensemble, (b) for the calculation of the projected density distribution, and (c) for the calculation of the radial density distribution.

with the external force. The function h characterizes the geometrical restriction of the consecutive chain segments. It is given by

$$h(\theta,\phi) = \cos^{-1}[\cos\theta\cos\gamma + \sin\theta\sin\gamma\cos\phi] \quad (26)$$

Together with the initial condition, i.e., the probability distribution of the first segment, which we choose to be characterized by a freely rotating first bond

$$G_1(\theta) \propto \exp\left(\frac{fb\cos\theta}{k_B T}\right)\sin\theta \quad (27)$$

Equation 24 determines the probability distribution uniquely for any i. The Gibbs partition function for a chain consisting of N segments in the fixed-force ensemble is given by

$$\Delta(N, f, T) = \int d\theta\, G_N(\theta) \quad (28)$$

from which the extension follows as

$$\langle R_z\rangle = k_B T \frac{\partial}{\partial f}\ln \Delta(N, f, T) \quad (29)$$

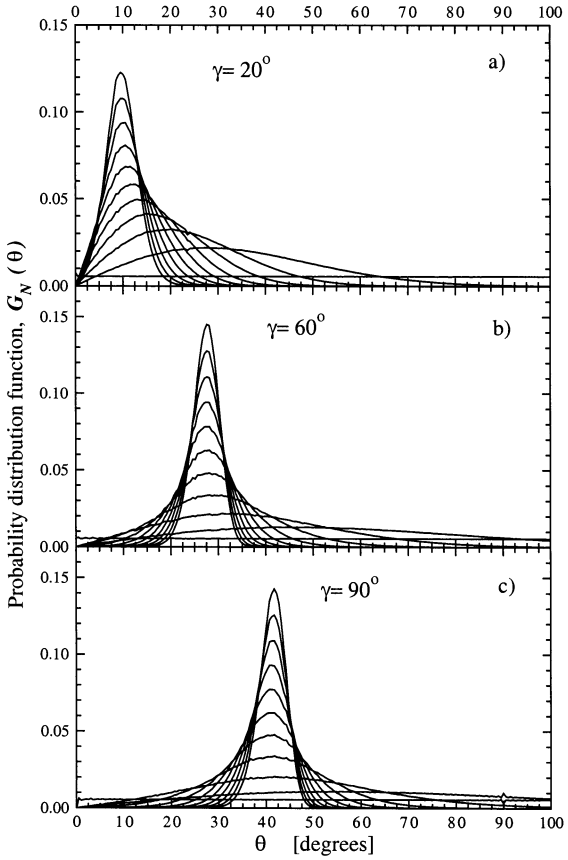

Figure 4. Probability distribution function of the angular orientation of the end chain bond with respect to the direction of the external force for chains with $N = 100$ and (a) $\gamma = 20°$, (b) $\gamma = 60°$, and (c) $\gamma = 90°$. The force values are $fb/k_BT = 0$, 1, 4, 9, 16, 25, 36, 49, 64, 81, and 100 (from bottom to top). The mesh parameter for all cases is $M_\theta = 5000$.

To solve the integral equation for the Green's function eq 24, we use a numerical iteration scheme which employs discretized coordinates. To that end, we divide the angular range of θ into M_θ equal intervals. To estimate the importance of discretization effects, we performed the entire procedure for various parameters M_θ. We found that the results for increasing resolution converge to a unique limit. This limit can be called the continuum limit because all results obtained for resolutions higher than a threshold resolution are practically independent of the M_θ parameter, and therefore identical to the results obtained if continuous angular coordinates were used. All computations have been performed on a 1 GHz Pentium IV with 512 MB memory and took a few minutes for chains with one hundred segments. As one can easily predict, the computational cost of the method increases linearly with the size of the chain.

The variation of the probability distribution function for the orientation of the last chain bond, $G_N(\theta)$ as a function of the applied force is shown in Figure 4 for chains consisting of $N = 100$ segments and bond angles $\gamma = 20$, 60, and 90°. All curves are normalized to render their integral to unity. The mesh parameter is fixed to $M_\theta = 5000$, which corresponds to the continuum limit as we will demonstrate later on. The force values are $fb/k_BT = 0$, 1, 4, 9, 16, 25, 36, 49, 64, 81, and 100 (with maxima from bottom to top, respectively). For better visualization of the region of interest, we show only the angular range θ = [0°, 100°]. Note the monotonic

increase of the maxima, accompanied by a decrease in the width of the curves as the force increases. At large forces, a sharp peak forms, with the most probable value of the angle close to $\theta \approx \gamma/2$, which is the angle of the all-trans configuration. Note that this value is however only slowly approached, since this completely straight configuration is totally devoid of configurational degrees of freedom and therefore entropically unfavorable. Clearly, for large values of the force, a very fine discretization of the angular variable is needed since the distribution becomes sharply peaked.

B. Transfer-Matrix Calculation of Spatial Distribution Functions. The formalism presented in the preceding section aims at calculating the average stretching of the chain as a function of the applied force via eq 29, but the information on the distribution function of chain extensions is lost. In this section we show how to calculate (i) the distribution of chain ends along the *z*-direction and (ii) the radial distribution of chain ends. The calculation of spatial distribution functions is much more involved. In case i, Green's function $G_i^z(\theta,z)$ in addition to the angle of the *i*th bond depends now also on the distance of the chain end from the origin along the *z*-axis. The geometry of the problem is depicted in Figure 3b. The integral equation eq 24 now also contains an integral over the *z* coordinate, and the transfer matrix is given by

$$\mathbf{T}^z(z,\theta;\, z',\theta') = \int_0^{2\pi} \mathrm{d}\phi\; \delta[\theta' - h(\theta,\phi)]\delta[z' - z - h_z(\theta,\phi)] \quad (30)$$

The function h is given by eq 26, while h_z reads

$$h_z(\theta,\phi) = b(\cos\theta\cos\gamma + \sin\theta\sin\gamma\cos\phi) \quad (31)$$

The initial condition for this case is

$$G_1^z(z,\theta) \propto \delta(z - b\cos\theta)\sin\theta \quad (32)$$

Once we have calculated $G_N^z(R_z,\theta)$, the Helmholtz partition function can be calculated as

$$Z_z(N,\, T,\, R_z) = \int_0^{\pi} \mathrm{d}\theta\; G_N^z(R_z,\theta) \quad (33)$$

from which the mean force acting on the chain end along the *z* direction follows as

$$\langle f\rangle = k_\mathrm{B}T\frac{\partial \ln Z_z(N,\, T,\, R_z)}{\partial R_z} \quad (34)$$

Note that the relations between the force and the extension in the fixed force ensemble, eq 29, and in the fixed extension ensemble, eq 34, are expected to give the same result only in the limit of infinite chain length $N \to \infty$. Since the calculation of the force-extension relation is much simpler in the fixed-force ensemble, we did not actually pursue the calculation of the force in the present fixed distance ensemble and always used the inverse relation eq 29 in the constant-force ensemble to obtain the distance-force curves. The normalized distribution of chain ends along the *z*-direction is given by

$$W_N^z(R_z) = \frac{Z_z(N,\, T,\, R_z)}{\int_0^{\infty} dR_z Z_z(N,\, T,\, R_z)} \quad (35)$$

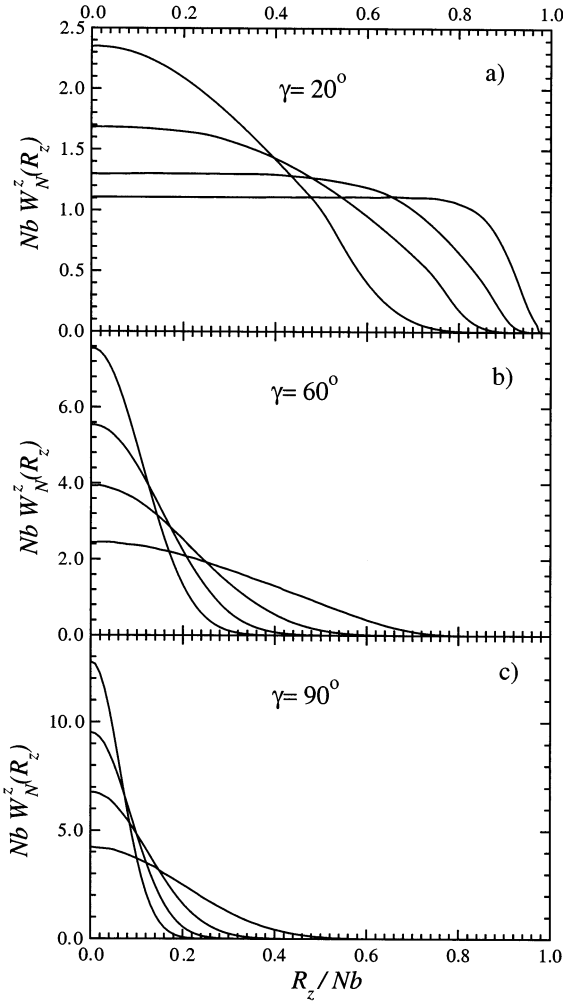

Figure 5. Projected end-point distribution function $W_N^z(R_z)$ for different values of the bond angle γ as indicated in the figure. From bottom to top at their maxima, the curves correspond to chain lengths $N = 10$, 25, 50, and 100.

Figure 5 displays the distribution function $W_N^z(R_z)$ calculated by eq 35 for the indicated values of bond angle. The curves correspond to chain lengths $N = 10$, 25, 50, 100 (becoming more sharply peaked around the origin with increasing chain length). The mesh parameters used here are $M_\theta = 100$ for the angular integration and $M_z = 200$ for the spatial integration.

For the radial Green function, $G_N^r(r,\theta)$, the transfer operator is

$$\mathbf{T}^r(r,\theta;\, r',\theta') = \int_0^{2\pi} d\phi\delta[\theta' - h_\theta(r,\, r')]\delta[r' - h_\mathrm{r}(r,\theta,\phi)] \quad (36)$$

where h_r is given by

$$h_r(r,\theta,\phi) = \sqrt{r^2 + b^2 + 2rb(\cos\theta\cos\gamma + \sin\theta\sin\gamma\cos\phi)} \quad (37)$$

and

$$h_\theta(r,\, r') = \cos^{-1}\left[\frac{(r')^2 + b^2 - r^2}{2rb}\right] \quad (38)$$

The initial condition corresponds to a freely rotating first bond and is given by

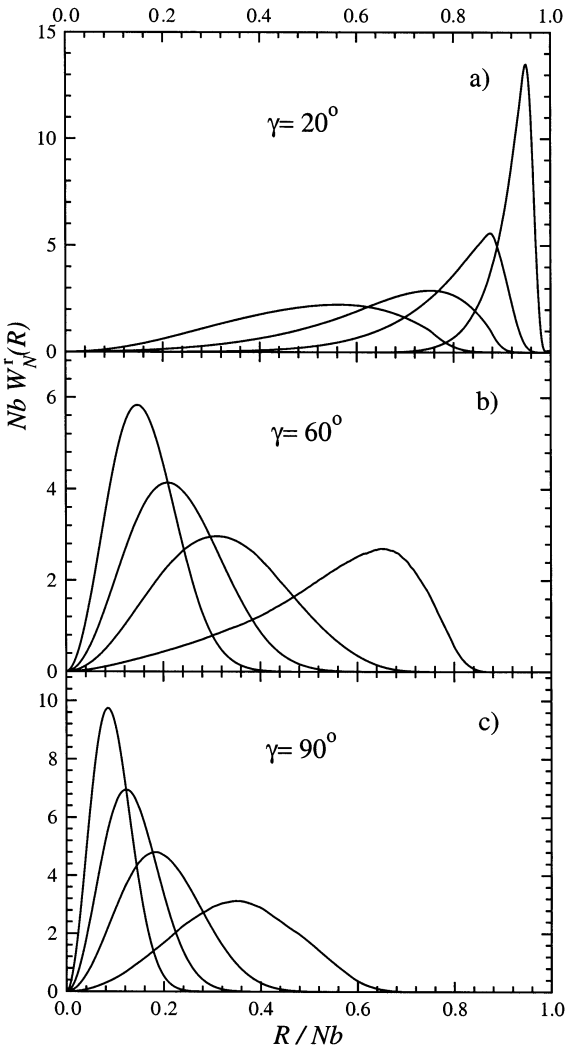

Figure 6. Radial distribution function $W_N^r(R)$, as determined by eq 41, for different values of bond angles as indicated in the figure. The different curves correspond to chain lengths $N = 10$, 25, 50, 100 (with the maximum moving to the left for increasing chain length).

$$G_2^r(r,\theta) = \delta[r - 2b\cos\theta]\delta[\theta - \gamma/2] \tag{39}$$

The radial unnormalized Green or partition function follows as

$$Z_r(N, T, R) = \int_0^\pi \mathrm{d}\theta\, G_N^r(R,\theta) \tag{40}$$

from which the normalized radial distribution function is obtained as

$$W_N^r(R) = \frac{Z_r(N, T, R)}{\int_0^\infty dR Z_r(N, T, R)} \tag{41}$$

In Figure 6, we display the radial distribution function $W_N^r(R)$ calculated according to eq 41 for selected values of the bond angle. From right to left in each panel, according to their maxima, the curves correspond to chain lengths $N = 10$, 25, 50, and 100. These quantities have been calculated with mesh parameters $M_\theta = 100$ and $M_r = 200$. Note the shift in the location of the maxima to smaller values of the radius as we increase the chain length, reflecting a loss in the stiffness of the chain. For instance, the chain with $N = 10$ and $\gamma = 20°$ is extremely stiff, with the radial distribution function being significantly different from zero only for R/Nb between 0.7 and 1, while for $N = 100$, the corresponding curve becomes much broader. In Figure 7, we compare our numerical results for $N = 100$, $\gamma = 20$, 60, and 90°, solid lines, with Gaussian distribution functions shown as broken lines

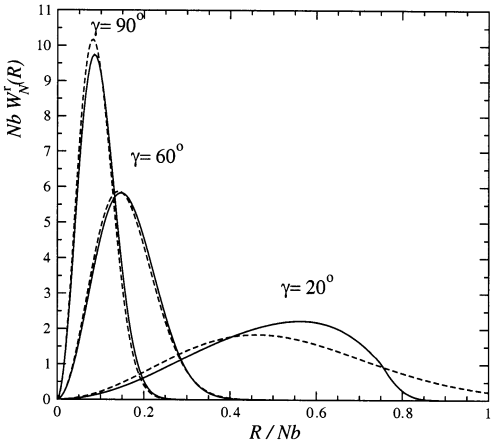

Figure 7. Comparison of numerical radial distribution functions (solid lines) for $N = 100$ and $\gamma = 20$, 60, and 90° with Gaussian-type distribution functions given by eq 42 (broken lines).

$$W_N^r(R) = \sqrt{\frac{54}{\pi}}\frac{R^2}{\langle R^2\rangle^{3/2}}\mathrm{e}^{-3R^2/2\langle R^2\rangle} \tag{42}$$

The mean squared end-to-end radius $\langle R^2\rangle$ was taken from eq 18. The agreement is quite good, especially for the larger bond angles, which shows that a FRC can be regarded as a FJC (as first noted by Kuhn) with an effective bond length a and an effective number of bonds $N_{\mathrm{eff}} = L/a$. For the smallest bond angle $\gamma = 20°$, the chain length is of the same order as the persistence length and therefore Gaussian behavior is not fully developed. Clearly, the distribution function of the FRC model for radial distances close to the maximal contour length shows pronounced and important deviations from the Gaussian behavior, but this is difficult to see from these plots. However, these are exactly the important deviations that are probed at large stretching forces and that lead to the nontrivial stretching response of these chain models, as will be the subject of the next section.

The relation between the radial distribution function, eq 41, and the projected distribution function, eq 35, can be written down as

$$W_N^z(z) = \int_0^\infty \mathrm{d}r\, 2\pi r\left[\frac{W_N^r(\sqrt{r^2+z^2})}{4\pi(r^2+z^2)}\right] \tag{43}$$

which we checked numerically. Note that the expression in the squared brackets is the probability to find the chain end at a certain distance along a fixed direction.

C. Results for the Stretching Response. In this section, we present our results for the stretching response of the FRC model and compare it with various analytical predictions. All transfer-matrix calculations are performed in the constant-force ensemble, and the chain extension is evaluated using eq 29 replacing the derivative by a finite difference.

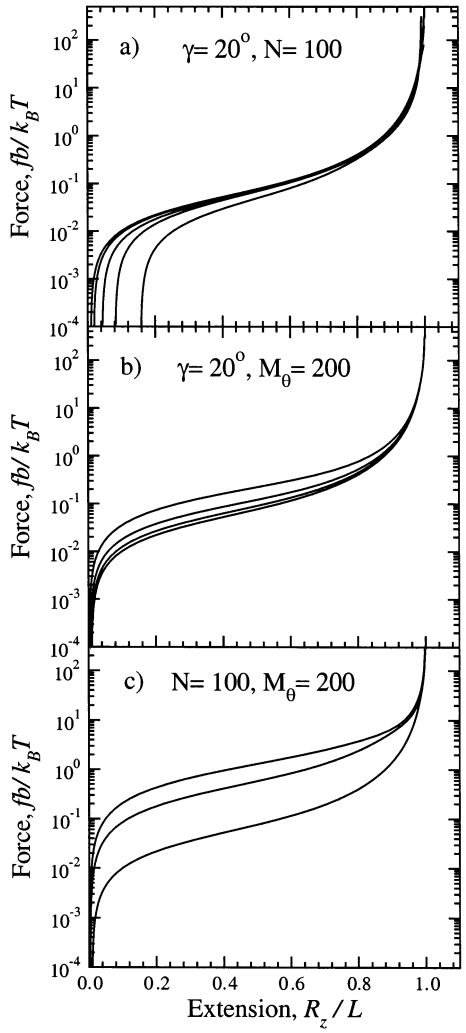

Figure 8. (a) Dependence of the force-extension curve on the mesh parameter M_θ, for fixed chain length and bond angle, $N = 100$, $\gamma = 20°$. From bottom to top, curves are for the values $M_\theta = 10$, 20, 40, 100, 200. (b) Dependence of the force-extension curve on the chain length at constant bond angle $\gamma = 20°$ and mesh parameter $M_\theta = 200$. From top to bottom curves are for the values $N = 10$, 25, 50, and 100. (c) Variation of the force-extension curve with the bond angle at constant chain length $N = 100$ and mesh parameter $M_\theta = 200$. From bottom to top curves are for $\gamma = 20$, 60, and 90°.

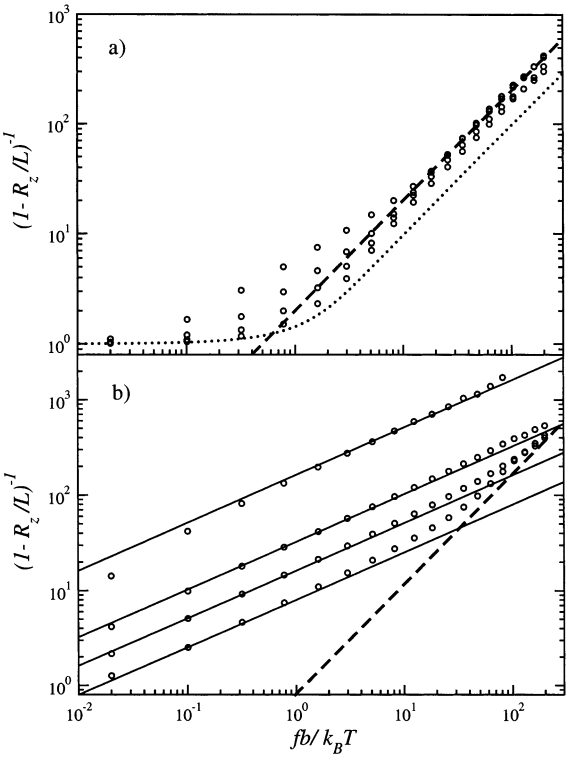

Figure 9. Force-extension relation on double-logarithmic axes for fixed mesh parameter $M_\theta = 400$ and chain length $N = 1000$. (a) Shown are rather large values of the bond angle $\gamma = 30$, 50, 70, and 90° (from top to bottom). The Langevin function, eq 13, for the FJC model is shown for comparison as a dotted line, while the thick dashed line denotes the limiting behavior in the discrete-chain limit as determined by eq 44. (b) Shown are small values of the bond angle $\gamma = 1$, 5, 10, and 20° (from top to bottom). For comparison, we show the corresponding analytical result in the strong stretching regime of the WLC model, eq 11, with the persistence length given by eq 22 (solid lines). The broken line denotes the discrete-chain limit as determined by eq 44.

In Figure 8, we present a compilation of raw data for the force-extension relation where we vary some of the parameters entering our computations. In all calculations, the stretching force has been tuned over a range of 6 orders of magnitude. In Figure 8a, we choose a fixed bond angle $\gamma = 20°$ and a fixed number of bonds $N = 100$ while we vary the number of angular mesh points M_θ, presenting data for $M_\theta = 10$, 20, 40, 100, 200 (from bottom to top). The curves practically overlap for values of M_θ greater than 200 (concluded from data not shown here), a trend that can be noticed already in the closeness of the curves with $M_\theta = 100$ and $M_\theta = 200$. In essence, such high values of M_θ are sufficient to reproduce the continuum limit, where the results are independent of the number of angular mesh points used. In Figure 8b, we show the variation of the stretching behavior for varying chain lengths $N = 10$, 25, 50, and 100 (from top to bottom) for fixed bond angle and mesh parameter. Again, the behavior of the force-extension curves is characterized by a limit—all curves tend to overlap for chain lengths larger that 100 (though for very stiff chains, that is small bond angles, one might need to go to much longer chains to eliminate finite-size effects, as we will discuss later on in more detail). Finally, in Figure 8c, we see the modification of force-extension curves for constant chain length $N = 100$ and mesh parameter $M_\theta = 200$, as a function of varying bond angle $\gamma = 20$, 60, and 90° (from bottom to top). As a qualitative trend, we see that chains with a smaller bond angle, which are therefore stiffer, yield more easily to an external force and show larger extension at fixed force.

In Figure 9, we present the force-extension curve in a slightly different form which enables us to compare the numerical result with the analytical large-force predictions for the WLC and FJC models, eqs 11 and 14. Namely, we plot$(1 - R_z/L)^{-1}$ vs fb/k_BT on double-logarithmic scales for a chain of length $N = 1000$ (finite-size effects will discussed separately later on). All results are calculated with a mesh parameter $M_\theta = 400$, which gives alawys an error smaller than the symbol size (and therefore negligible for the present purpose). In Figure 9a, we display the results for large values of bond angle $\gamma = 30$, 50, 70, and 90° (corresponding to circles from top to bottom, respectively), while in Figure 9b the curves for small bond angles are shown, $\gamma = 1$, 5, 10, and 20° (from top to bottom). The Langevin function, which is the exact force-stretching relation for

the FJC model, eq 13, is displayed for comparison in Figure 9a as a dotted line. Note that in the large-force regime (which for the FRC model is realized for $fb/k_BT > \ell/b$), the computed curves are close to the Langevin curve, that is their slope is very close to 1. In the intermediate force regime, the data show deviations from the Langevin curve, which become more pronounced as the bond angle decreases. For small bond angles, i.e., for rather stiff chains, we expect the behavior of the FRC model to be similar to the one of the WLC model. Accordingly, we show in Figure 9b straight lines representing the large-force behavior of the WLC model, given by eq 11, with a persistence length calculated by the use of eq 22 for the four bond angles $\gamma = 1$, 5, 10, and 20°. The agreement is excellent (except for the topmost curve with a bond angle of $\gamma = 1°$ and a persistence length of $\ell/b \approx 6565$ which exceeds the length of the chain $L \approx 1000$), which shows that indeed the WLC describes the stretching behavior of the FRC model for forces $b/\ell < fb/k_BT < \ell/b$. Note that the large-force behavior shows distinct deviations from the Langevin formula and is in fact quite accurately described by the curve

$$(1 - R_z/L)^{-1} = \frac{cfb}{k_BT} \tag{44}$$

with $c = 2$, which differs from the asymptotic Langevin result eq 14 by a factor of 2 and is shown as a thick dashed line. The reason for the difference lies in the fact that a strongly stretched FRC shows rotational fluctuations only in a plane (i.e., it has only one angular degree of freedom), whereas the FJC shows angular fluctuations in two directions. The difference in dimensionality of the conformation subspace accounts for the difference by a factor of 2, as is explained in detail in Appendix B.

In Figure 10, we investigate in more detail the effects of finite-chain length, which are especially pronounced for stiff chains (small bond angles). We show $(1 - R_z/L)^{-1}$ vs fb/k_BT in logarithmic axes for small bond angles $\gamma = 1$, 5, 10, and 20° in Figure 10a−d, respectively. In each part, data for chain lengths $N = 10$, 100, 1000, and 2000 are presented and compared with the heuristic fit formula eq 12 (solid lines) which had been shown to accurately describe the WLC stretching behavior for all forces. The mesh parameter is set to $M_\theta = 1000$ for all the results displayed. The persistence lengths for the bond angles $\gamma = 1$, 5, 10, and 20° follow from eq 22 as $\ell/b = 6565$, 262, 64, and 15, respectively. At a force $fb/k_BT \sim b/\ell$, which describes the crossover from the linear force regime to the nonlinear force regime, the external force is strong enough to orient persistent segments along the force direction. Therefore, finite-size effects in the nonlinear force regime are only noticeable if the persistence length is larger than the chain length. Accordingly, in Figure 10d with a persistence length of $\ell = 15$ only the results for a a monomer number $N = 10$ show finite-size effects, while in Figure 10a with a persistence length of $\ell = 6565$ all chain lengths studied are subject to finite-size effects (and the infinite-length limit, denoted by the solid line, is not reached with the finite-length chains studied here). As can be seen, however, finite size effects are stronger for smaller forces. This can be understood by using the scaling relation for the deflection length, eq 16: Finite-size effects are expected to become irrelevant if the deflection length is smaller than the chain length, which corresponds to

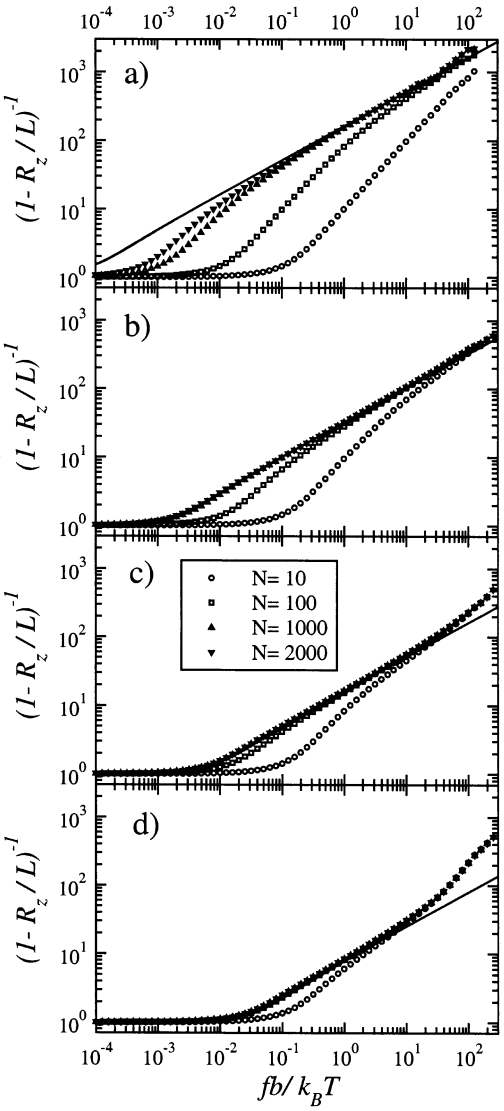

Figure 10. Finite-size analysis of the force-extension data in the intermediate force range. The mesh parameter M_θ is maintained at a reliably high value of 400. The four parts correspond from top to bottom to bond angles $\gamma = 1$, 5, 10, and 20° giving rise to persistence lengths of $\ell/b = 6565$, 262, 64, and 15, respectively. As indicated in the legend the chain lengths are $N = 10$, 100, 1000, 2000. The solid lines denote the WLC prediction according to the fit formula, eq 12. Deviations for small forces are due to finite-size effects, deviations for large forces in parts c and d are due to the crossover to the discrete-chain regime.

$$\frac{fb}{k_BT} > \frac{b/}{L^2} \tag{45}$$

For the data in Figure 10a with a persistence length $\ell = 6565$, this means that finite size effects for the chains of a length $L = 2000$, 1000, 100, and 10 should become irrelevant for forces larger than $fb/k_BT = 0.0015$, 0.006, 0.6, and 60, which is of the order of what we observe in the numerical data. We note that the deviations between the data and the solid lines for large forces in Figure 10c,d are due to the crossover to the DC regime, as discussed before.

We next scrutinize the linear small-force regime, which is governed by the relation eq 10, which involves

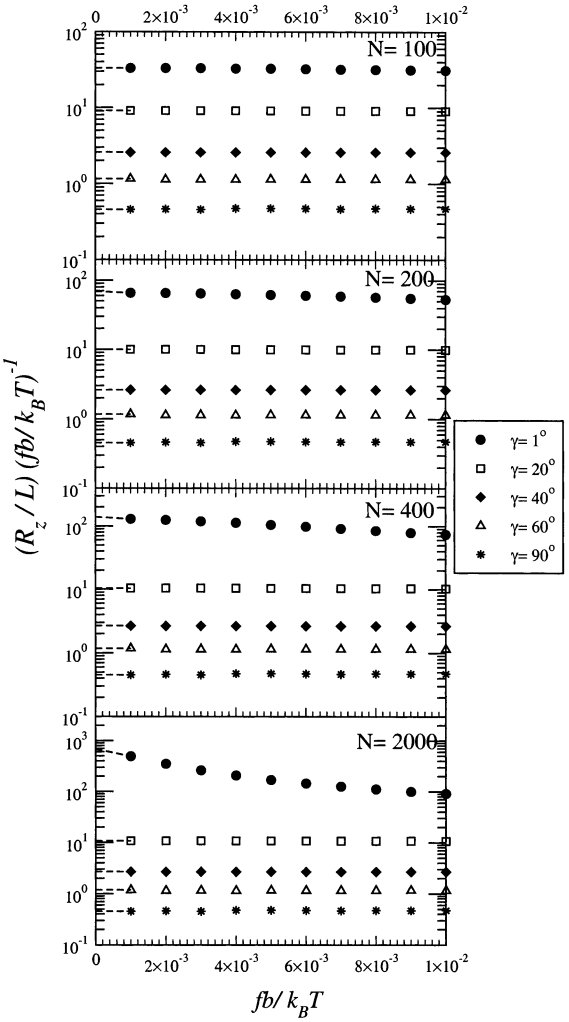

Figure 11. Analysis of the force-extension curves in the small-force regime. Shown is the chain extension divided by the force, $(R_z/L)(fb/k_BT)^{-1}$, as a function of the force. A few representative bond angles are chosen and the chain length is increased from 100 to 2000 (from upper to lower panel). The extrapolation of the data to zero force is indicated by dashed lines.

the Kuhn length a. In Figure 11, we plot the quantity $(R_z/L)(fb/k_BT)^{-1}$ as a function of the force for various chains lengths and bond angles, which, according to eq 10, for an infinitely long chain in the small-force regime should be equal to $(R_z/L)(fb/k_BT)^{-1} \simeq a/3b$. By extrapolating our data to the limit of zero force, as denoted by broken lines in Figure 11, we are therefore able to extract the Kuhn length a. In Figure 12, we plot our zero-force extrapolation estimates for $(R_z/L)(fb/k_BT)^{-1}$ for the different chain lengths used together with the analytical prediction for the FRC model eq 21 (solid line). The agreement is excellent except for short chains and small bond angles. The reason is simple to understand. For a FRC to exhibit the linear force regime, the chain has to consist of many uncorrelated segments; i.e., the length L of the chain has to be much larger than the persistence length ℓ. With the persistence lengths for the four smallest bond angles considered, $\gamma = 1$, 5, 10, and 20°, leading via eq 22 to $\ell/b = 6565$, 262, 64, and 15, we understand the marked crossover shown in Figure 12. Much longer chains would be needed to see the linear regime for these stiff chains.

We summarize our numerical results in Figure 13. All data have been obtained with chains consisting of $N = 1000$ bonds. Figure 13a shows the rescaled stretching R_z/L as a function of the rescaled force fb/k_BT on double logarithmic scales for bond angles $\gamma = 10$, 20, 30, 50, and 70° (from top to bottom) in the small-force regime. The solid lines indicate the linear asymptotic behavior according to eq 10 with a Kuhn length given by eq 21. In Figure 13b, the intermediate force regime is covered. We show data for bond angles $\gamma = 1$, 5, 10, 20, 30, and 50° (top to bottom) together with the large-force prediction of the WLC model, eq 11, with a persistence length determined by eq 22. The deviations from the WLC prediction for the bottom curve follow from the limited range of forces where the WLC prediction is expected to be valid, according to eq 23, since the persistence length for this chain is quite low. The deviation from the WLC model for the topmost chain ($\gamma = 1°$) is due to finite-size effects, as has been discussed before. Figure 13c compares the stretching response for all different bond angles considered with the large-force prediction eq 44. According to the scaling prediction eq 23 a chain with a bond angle $\gamma = 10°$ and persistence length $\ell/b = 64$ should crossover from the WLC prediction to the large-force regime at a force $fb/k_BT \sim \ell/b \simeq 64$, in rough agreement with what is seen in Figure 13c. Accordingly, the data for $\gamma = 5°$ should cross over at $fb/k_BT \sim \ell/b \simeq 262$, and the data for $\gamma = 1°$ should cross over at $fb/k_BT \sim \ell/b \simeq 6565$ (outside the force range considered by us).

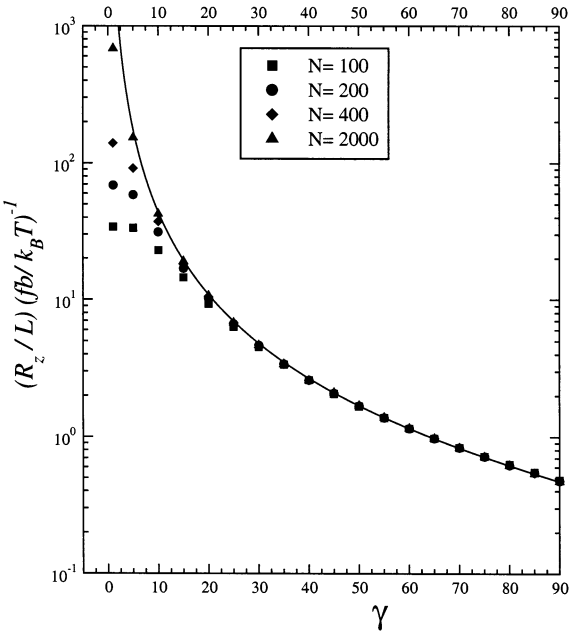

Figure 12. Slope of the force-extension relation in the limit of zero force as determined in Figure 11 as a function of the bond angle for different chain lengths. The analytical result (continuous line) in the infinite-chain limit, $N \to \infty$, eqs 21 and 10, is displayed for comparison.

In summary, the stretching response of the FRC shows three distinct scaling ranges, very similar to the prediction of the scaling analysis of section II, which are given by

$$\frac{R_z}{L} \simeq \begin{cases} \dfrac{fa}{3k_BT} & \text{for } \dfrac{fb}{k_BT} < \dfrac{b}{\ell} \\ 1 - \left(\dfrac{f\ell}{4k_BT}\right)^{-1/2} & \text{for } \dfrac{b}{\ell} < \dfrac{fb}{k_BT} < \dfrac{\ell}{b} \\ 1 - \left(\dfrac{fb}{ck_BT}\right)^{-1} & \text{for } \dfrac{\ell}{b} < \dfrac{fb}{k_BT} \end{cases} \qquad (46)$$

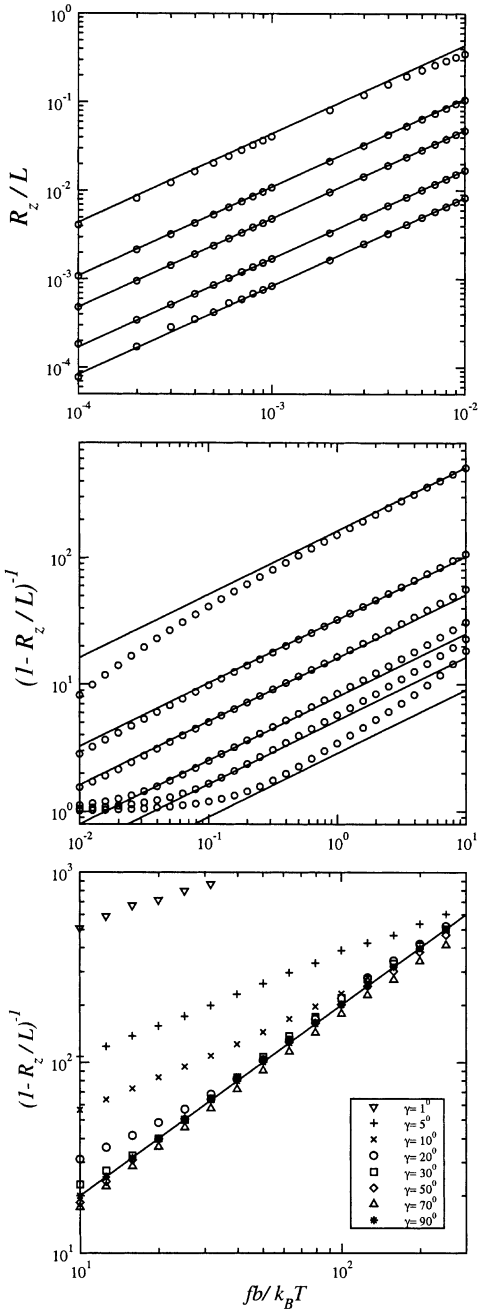

Figure 13. Summary of the numerical results (for a chain consisting of $N = 1000$ bonds) in comparison with analytical predictions in the various force regimes. (a) In the linear small-force regime, the force-extension curve for the FRC model is accurately described the linear prediction eq 10 (solid lines). The data correspond to (from top to bottom) $\gamma = 10$, 20, 30, 50, and 70°. (b) In the intermediate-force regime, the force-extension data for the FRC are well described by the large-force limit of the WLC model, as given by eq 11. The circles represent numerical results for $\gamma = 1$, 5, 10, 20, 30, and 50° (from top to bottom). (c) In the large-force limit the data ($\gamma =$ 1, 5, 10, 20, 30, 50, 70, and 90° from top to bottom) approach the discrete chain limit as given by eq 44.

For the FRC model, the constant c is given by $c = 2$; for the EJC model considered in section II this constant was found to be unity. In the general case, this constant depends on the architecture of the joints connecting different chain segments and will lie between one and two, as is explained in more detail in Appendix B.

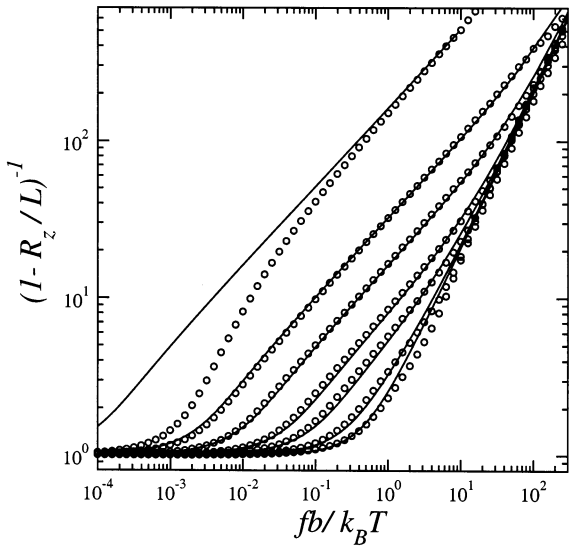

Figure 14. Global fit of the numerical force-extension data for FRC in the long chain limit ($N = 1000$). The circular symbols represent computational results for different bond angles $\gamma = 1$, 5, 10, 20, 30, 50, and 70° (from top to bottom) while the continuous curves are derived from the fitting function eq 49 with $\beta = 2$, $c = 2$, and $\tilde{\gamma} = \infty$ (inextensible chain). The deviation of the topmost curve ($\gamma = 1°$) is due to finite-size effects.

IV. Discussion

Our most important finding is that a semiflexible chain which consists of some type of discrete segments will cross over to a novel discrete-chain (DC) scaling range for large forces. In this DC regime, the stretching response is similar (though not identical) to the large-force regime of the FJC model, which can be understood as a result of a force-induced decoupling between adjacent chain segments. Experimentally, this will have profound consequences for the fitting of stretching data of polymers in the large-force regime. To make such experimental comparison feasible, we now present a simple fitting function which is valid for the entire force range. First of all, we observe that the WLC stretching formula, eq 12, can be written as

$$\frac{f\ell}{k_B T} = F_{\mathrm{WLC}}[(1 - R_z/L)^{-1}] \tag{47}$$

with the function $F_{\mathrm{WLC}}[x]$ defined as

$$F_{\mathrm{WLC}}[x] = \frac{3}{4} - \frac{1}{x} + \frac{x^2}{4} \tag{48}$$

The proposed global fitting function for the force response of a discrete semiflexible chain is

$$R_z/L = 1 - \{(F_{\mathrm{WLC}}{}^{-1}[f\ell/k_B T])^{\beta} + (cfb/k_B T)^{\beta}\}^{-1/\beta} + f/\tilde{\gamma} \tag{49}$$

which has the desired property that for large forces the stretching is given by eq 44 while for smaller forces the WLC behavior in eq 11 is reproduced. The sharpness of the crossover between these two limits is controlled by the parameter β. Note that the function $F_{\mathrm{WLC}}{}^{-1}[x]$ is the functional inverse of $F_{\mathrm{WLC}}[x]$. In eq 49 we added a linear stretching term which is characterized by the stretching modulus $\tilde{\gamma}$ of the chain. For saturated carbon backbones, the modulus was derived from quantum-chemical ab

initio calculations and found to be of the order of $\tilde{\gamma} = 28$ nN.[23] In Figure 14, we compare our numerical data for $N = 1000$ and various bond angles $\gamma = 1$, 5, 10, 20, 30, 50, and 70° (top to bottom) with the fit function eq 49 for parameter values $\beta = 2$, $\tilde{\gamma} = \infty$ (inextensible chain), and $c = 2$. The agreement is satisfactory over the entire range of forces. The deviations seen for the top curve with $\gamma = 1°$ are due to finite size effects and not to a break down of our fitting procedure. Therefore, in an experimental test of our predictions for the crossover to the discrete chain regime for large forces, we suggest usage of the function in eq 49 with a crossover parameter $\beta = 2$. For a chain consisting of freely rotating chemical bonds with fixed bond angles (such as a fully saturated carbon backbone) we suggest to use $c = 2$, for bonds that are isotropic we suggest the vaule $c = 1$. Preliminary comparison of experimental extension-force data for single poly(vinylamine) chains with our fit function show good agreement and in specific allow to describe the high-force regime more accurately than the wormlike chain model does.[24]

Factors that have not been studied by us include the torsional bond potential due to interactions between chemical groups on further-nearest neighbor monomers, which become important for example for PEG polymers. Such interactions have recently been derived from ab initio calculations.[25] To gain more detailed understanding of the effects of such factors, the methods used in this paper are currently generalized to the case of additional torsional potentials. We find that in a coarse-grained fashion, such effects can be implicitly taken into account by choosing a suitable persistence length, while the qualitative features discussed here, most notably the occurrence of the discrete-chain regime and the functional form of the crossover function, are not altered.[24] One other possible source of inaccuracy is an increase of the effective bond length and a decrease of the bond angle at large stretching forces. Quantum-mechanical ab initio calculations indeed show that the bond length of a fully saturated carbon-backbone chain changes by less than 1% and the bond angle by about 2% as one goes from zero force to a force of 1 nN.[24] Such effects can thus be safely neglected.

Furthermore, interactions between monomers such as excluded-volume interactions or charge−charge interactions have not been considered. It has been shown, however, that the charge−charge interactions can be taken into account by assuming a force-dependent persistence length.[23] A scaling function for this effective persistence length, which takes salt-screening effects into account, has been given[23] and could be directly included into our fitting function, eq 49. However, it is to be noted that those effects are smaller than the discretization effects discussed in this paper. Excluded volume effects, leading to chain swelling, modify the linear stretching response, eq 10, and lead to a nonlinear stretching-force relation. These effects are however only relevant for very small forces and therefore will not effect our results and predictions in any way. Finally, the way the linear stretching term $f/\tilde{\gamma}$ has been added into the extension function in eq 49 is ad-hoc and demands critical discussion. It has been shown that coupling terms between elongational fluctuations and bending fluctuations are present but quite small for large elongational moduli $\tilde{\gamma}$, which is the case for carbon backbones.[23] Also, there are anharmonic corrections to the linear stretching law assumed in eq 49, but the next-leading correction terms have been derived from quantum-chemical ab initio calculations and have been found to be negligible for typical forces that can be probed in AFM experiments.[23] In essence, the fitting function in eq 49 should serve as a quite reliable recipe to understand experimental data for synthetic or other freely rotating polymer chains.

Acknowledgment. Stimulating discussions with H. Gaub, T. Hugel, I. Jäger, and M. Seitz are acknowledged. L.L. would like to thank the Killam Trusts at Dalhousie University for support offered through a Killam Scholarship. R.R.N. acknowledge financial support by Deutsche Forschungsgemeinschaft (DFG, SFB 486) and the Fonds der Chemischen Industrie.

Note Added in Proof. A similar discrete worm-like chain model has recently been studied in two dimensions, see Lamura, A.; Burkhardt, T. W.; Gompper, G. *Phys. Rev. E: Stat. Phys., Plasmas, Fluids, Relat. Interdiscip. Top.* **2001**, *64*, 061801.

Appendix A. A Model for the Stiffness of Globular Biopolymers

In this appendix we propose a simple way of calculating the stiffness ϵ of the EJC model for polymers whose buildings blocks have a certain width and are stabilized by some type of harmonic bonds. The model we propose applies to a large class of biopolymers made of globular subunits, such as actin or tubulin, and consists of rectangular subunits of length b and width d which are connected at the joint edges by flexible bonds, i.e., hydrogen bonds; see Figure 1c. This model might also apply to α-helices, since each turn of this helix can move rather independently from the other turns due to the large number of rotating bonds. Denoting the spring constant of one hydrogen bond by k_BTK, and assuming that there are M hydrogen bonds at each edge, the stiffness of one joint can for small bending angles be written as

$$\epsilon \simeq Kd^2M$$

From our result in eq 9, valid for stiff joints, we find the persistence length

$$\ell \simeq KMd^2b \tag{A1}$$

which scales with the volume $v = d^2b$ of the segments. This scaling is fundamentally different from the case of elastic rods, where the bending rigidity is proportional to the fourth power of the rod diameter.[26] A rough estimate for K is $K \approx 200$ nm^{-2}, based on a bond length of ≈ 0.2 nm and a binding energy of k_BT. For an α-helix we assume $M = 2$ and $b \approx d \approx 0.4$ nm, which gives a persistence length of $\ell \approx 25$ nm. This is in rough agreement with previous estimates.[27] For tubulin, we obtain with $d \approx 25$ nm, $b \approx 4$ nm, and $M = 4$, the value $\ell \approx 2$ mm, which agrees qualitatively with the experimental value of $\ell \approx 5$ mm.[28] For actin, we obtain with $d \approx b \approx 5.5$ nm and $M = 1$ the value $\ell \approx 30\mu m$, which agrees surprisingly well with experimental results.[29] We note that the largest indeterminant in our estimates is the number of hydrogen bonds involved in the joint stabilization, but the qualitative scaling of the persistence length with the segment volume seems to be correct.

Appendix B. Stretching Response in the Discrete-Chain Limit

1. Standard Case: FJC in Three Dimensions. Before we calculate the force response of a freely rotating chain in the large-force limit, we will repeat the calculation for the stretching-force relation for the freely jointed-chain model, a calculation that leads to the classical Langevin equation. Since all bonds decouple from each other, it is sufficient to consider a single bond subject to an external force f. The partition function Z reads

$$Z = \int_0^{2\pi} \frac{d\phi}{2\pi} \int_0^{\pi} \frac{d\theta \sin\theta}{2} e^{fb\cos(\theta)/k_B T} \tag{B1}$$

where ϕ is the torsional angle (which rotates freely and can be integrated out) and θ is the bond angle measured with respect to the direction of the external force. The final result is

$$Z = \frac{2\pi}{fb/k_B T}(e^{fb/k_B T} - e^{-fb/k_B T}) \tag{B2}$$

from which the stretching response of a single bond follows as

$$\frac{\langle z\rangle}{b} = \frac{\partial \ln Z}{\partial bf/k_B T} = \frac{1 + e^{-2fb/k_B T}}{1 - e^{-2fb/k_B T}} - \frac{1}{fb/k_B T} \tag{B3}$$

This is the classical Langevin formula (compare with eq 13), which for large forces can be written as

$$\frac{\langle z\rangle}{b} \le 1 - \frac{1}{fb/k_B T} \tag{B4}$$

(compare with eq 14).

2. FRC in the Large Force Regime. A freely rotating chain in the large force regime assumes an all-trans configuration, and each bond performs angular fluctuations which are confined to a cone. The orientation of this cone depends on the bond angle. For the following calculation, we make the simplifying assumption that each bond rotates independently from the adjacent bonds within a fixed cone; i.e., we neglect correlations between neighboring bonds. The partition function for a single bond reads

$$Z = \int_0^{\pi} \frac{d\phi}{\pi} e^{fb[t+(s-t)\cos(\phi)]/k_B T} \tag{B5}$$

where ϕ is the torsional angle. The orientation and geometry of the cone is contained in the coefficients t and s, where $s = \cos(\gamma/2)$ is the ratio of the projected bond length and the true bond length in the all-trans configuration. The coefficient t is a measure of the opening width of the cone and is irrelevant for the following calculation, as will turn out later on. For large forces, we can expand the cosine in the exponential and obtain

$$Z \simeq \sqrt{\frac{1}{2\pi fb(s - t)/k_B T}} e^{fbs/k_B T} \tag{B6}$$

By taking a derivative with respect to the external force, we obtain the result for the orientation of a single bond, valid in the large-force regime

$$\frac{\langle z\rangle}{sb} = \frac{\partial \ln Z}{\partial sbf/k_B T} \simeq 1 - \frac{1}{2sfb/k_B T} \tag{B7}$$

The dependence on the geometric factor t has indeed dropped out, as announced. One notes the factor of $2s = 2\cos(\gamma/2)$ in eq B7 as compared to the standard result for the FJC model eq B4. This difference can be interpreted as an enhancement of the external force, which is easily understood since fluctuations (which work against the external force) are weakened due to the restricted dimension available for fluctuations. As can be seen from the numerical results in Figure 9, the factor $2\cos(\gamma/2)$ is relevant when it comes to describing stretching data (and will also be relevant for the interpretation of experimental data) and is represented by the parameter c within our fitting function eq 49. For small bond angles, one can replace this factor by the limiting value $c \approx 2$, which corresponds to the thick broken line in Figure 9.

References and Notes

(1) Clausen-Schaumann, H.; Seitz, M.; Krautbauer, R.; Gaub, H. E. *Curr. Opin. Chem. Biol.* **2000**, *4*, 524.
(2) Smith, S. B.; Finzi, L.; Bustamente, C. *Science* **1992**, *258*, 1122.
(3) Bustamente, C.; Marko, J. F.; Siggia, E. D. *Science* **1994**, *265*, 1600.
(4) Vogolodskii, A. *Macromolecules* **1994**, *27*, 5623.
(5) Odijk, T. *Macromolecules* **1995**, *28*, 7016.
(6) Marko, J. F.; Siggia, E. D. *Macromolecules* **1995**, *28*, 8759.
(7) Ha, B. Y.; Thirumalai, D. *J. Chem. Phys.* **1997**, *106*, 4243.
(8) Rief, M.; Clausen-Schaumann, H.; Gaub, H. E. *Nature: Struct. Biol.* **1999**, *6*, 346.
(9) Rief, M.; Gautel, M.; Oesterhelt, F.; Fernandez, J. M.; Gaub, H. E. *Science* **1997**, *276*, 1109.
(10) Rief, M.; Oesterhelt, F.; Heymann, B.; Gaub, H. E. *Science* **1997**, *275*, 1295.
(11) Oesterhelt, F.; Rief, M.; Gaub, H. E. *New J. Phys.* **1999**, *1*, 6.
(12) Ortiz, C.; Hadziioannou, G. *Macromolecules* **1999**, *32*, 780.
(13) Hugel, T.; Grosholz, M.; Clausen-Schaumann, H.; Pfau, A.; Gaub, H.; Seitz, M. *Macromolecules* **2001**, *34*, 1039.
(14) Leger, J. F.; Romano, G.; Sarkar, A.; Robert, J.; Bourdieu, L.; Chatenay, D.; Marko, J. F. *Phys. Rev. Lett.* **1999**, *83*, 1066.
(15) Kovac, J.; Crabb, C. C. *Macromolecules* **1982**, *15*, 537.
(16) Moroz, J. D.; Nelson, P. *Proc. Natl. Acad. Sci. U.S.A.* **1997**, *94*, 14418.
(17) Bouchiat, C.; Wang, M. D.; Allemand, J. F.; Strick, T.; Block, S. T.; Croquette, V. *Biophys. J.* **1999**, *76*, 409.
(18) Fixman, M.; Kovac, J. *J. Chem. Phys.* **1973**, *58*, 1564.
(19) Odijk, T. *Macromolecules* **1983**, *16*, 1340; **1984**, *17*, 502.
(20) Flory, P. J. *Statistical Mechanics of Chain Molecules*; Hanser Verlag: München, Germany, 1989.
(21) Grosberg, A. Yu.; Khokhlov, A. R. *Statistical Physics of Macromolecules*; AIP Press: New York, 1994.
(22) Kostrowicki, J.; Scheraga, H. A. *Comput. Polym. Sci.* **1995**, *5*, 47.
(23) Netz, R. R. *Macromolecules* **2001**, *34*, 7522.
(24) Hugel, T.; Seitz, M.; Gaub, H.; Livadaru, L.; Netz, R. R.; Kreuzer, H. J. To be published.
(25) Kreuzer, H. J.; Wang, R. L. C.; Grunze, M. *New J. Phys.* **1999**, *1*, 1.21.
(26) Landau; Lifshitz. *Theory of Elasticity*; Pergamon Press: Oxford, England, 1986.
(27) Vogel, H.; Nilsson, L.; Rigler, R.; Voges, K.-P.; Jung, G. *Proc. Natl. Acad. Sci. U.S.A.* **1988**, *85*, 5067.
(28) Gittes, F.; Mickey, B.; Nettleton, J.; Howard, J. *J. Cell Biol.* **1993**, *120*, 923.
(29) Ott, A.; Magnasco, M.; Simon, A.; Libchaber, A. *Phys. Rev. E* **1993**, *48*, R1642.

MA020751G